Photoionization and Auger decay of the 3*d* vacancy state of atomic strontium: Electron-electron correlations

J. Nikkinen,[1,2,*] H. Aksela,[1] S. Fritzsche,[2] S. Heinäsmäki,[1] R. Sankari,[1] E. Kukk,[1,3] N. Berrah,[4] and S. Aksela[1]
[1]*Department of Physical Sciences, University of Oulu, P.O. BOX 3000, FIN-90014 University of Oulu, Finland*
[2]*Department of Physics, University of Kassel, Heinrich-Plett-Straße 40, D-34132 Kassel, Germany*
[3]*Department of Physics, University of Turku, FIN-20014 Turku, Finland*
[4]*Department of Physics, Western Michigan University, Kalamazoo, Michigan 49008-5151, USA*
(Received 25 May 2005; published 11 October 2005)

The 3*d* photoionization and subsequent normal Auger decay processes in atomic strontium have been investigated. To understand the electron spectra following photoionization of a 3*d* electron, a series of *ab initio* computations, based on the multiconfiguration Dirac-Fock method, were performed. From the calculated photoionization and Auger decay amplitudes the relative photoionization cross sections were derived, together with the total and partial Auger decay widths and relative Auger intensities. Emphasis was placed on the effects of electron-electron correlations in the 3*d* hole state. The theoretical predictions were compared to the high-resolution synchrotron radiation-induced photoelectron and Auger electron spectra.

DOI: 10.1103/PhysRevA.72.042706 PACS number(s): 32.80.Fb, 32.80.Hd

I. INTRODUCTION

Many detailed investigations exist for core photoionization and subsequent normal Auger decay processes in free alkaline earth metal atoms (see, e.g., Refs. [1–7]). In the past, the main motivation for these studies arose from the high sensitivity of the core ionized states to the effects of electron-electron correlations. In most of these spectra, a strong influence could be assigned to the relaxation ("collapse") of the unoccupied ground state orbitals in the course of the ionization process. These investigations showed, in particular, that configuration interaction has to be taken into account in order to understand the complexity of the core-level photoelectron and Auger electron spectra.

In our previous work [7], the Ba 4*d* photoionization and the subsequent Auger decay process resulting in valence double hole state (v^{-2}) were studied by performing a series of multiconfiguration Dirac-Fock (MCDF) calculations. We noticed that although we were able to generate, within certain configuration expansions for the 4*d* hole state, the structures seen in the photoelectron spectrum (PES), the predictions for the subsequent Auger electron spectrum (AES) failed drastically. This was because the details of the AES appeared to be more sensitive to the orbital collapse following 4*d* ionization than those of the PES. By performing the MCDF calculations for the 4*d* hole state in two steps, first with smaller configuration expansion to obtain good approximations for the inner-shell orbitals and then expanding the configuration set and keeping the inner-shell orbitals frozen from the first calculation, the theoretical AES was found to be in good agreement with the spectrum observed experimentally. Similar effects of relaxation and the collapse of the 4*d* orbital can be expected for the Auger decay of the 3*d* hole state of strontium following 3*d* photoionization.

Up to the present, only very few experimental or theoretical results have been reported for Sr 3*d* photionization and subsequent Auger decay processes. In the 1970s, Mehlhorn *et al.* [1] investigated experimentally the Sr 3*d* AES using electron excitation. However, the resolution and statistics of that spectrum were modest, which did not allow any precise analysis of the Auger decay. We recently measured synchrotron radiation-induced Sr 3*d* PES and modeled it using the MCDF calculations [6]. However, our calculations in Ref. [6] did not adequately reproduce the structures seen in the PES. With respect to our previous study, in this paper we have recalculated the Sr 3*d* PES using slightly different configuration expansions in the 3*d* hole state. In order to better see the effects of electron-electron correlations in the 3*d* hole state, we have also studied in detail the subsequent Auger decay processes resulting in the $4p^{-2}$, $4s^{-1}\,v^{-1}$, $4p^{-1}\,v^{-1}$, and v^{-2} final ionic configurations.

II. EXPERIMENT

The experiment for gas phase Sr 3*d* PES, induced with photon energy of 255 eV, has been discussed in Ref. [6]. The AES measurements were carried out at the gas phase beamline I411 at MAX II storage ring in Lund, Sweden [8,9]. A resistively heated oven was used to produce an intense atomic beam of Sr in the collision area. The operating temperature of the oven was in the range of 450–530 °C, corresponding to a Sr vapor pressure of about 10^{-3}–10^{-2} mbar in the crucible. The ejected Auger electrons were recorded with a rotatable SES-100 hemispherical electron analyzer at the emission angle of 54.7° relative to the polarization axis of the linearly polarized light. The energy scale and transmission correction [10] of the analyzer were determined using the well known Xe $N_{4,5}OO$ Auger [11] and Xe 4*d* photoelectron lines [12].

The actual measurements were performed in three parts. First, the photon energies 190 and 210 eV were used to measure the respective kinetic energy ranges of 60–110 and 95–135 eV of the AES. Different photon energies were chosen for different energy ranges to avoid overlap of the Sr

*Electronic address: juha.nikkinen@oulu.fi

photoelectron lines with the AES. No changes in the relative Auger electron intensities were observed between the measurements in the kinetic energy range of 95–110 eV, which was recorded in both measurements. Instrumental resolution of about 250 meV at full width of half-maximum (FWHM) was used in these measurements. In addition, the region of the $4p^{-1}v^{-1}$ final ionic states of the Auger decay (E_k =95–110 eV) was recorded using the photon energy of 200 eV with the instrumental resolution of about 50 meV at FWHM.

III. THEORY

The relative photoelectron and Auger electron intensities have been calculated using a two-step model. In this model the primary 3*d* photoionization of the Sr atom is assumed to take place independently of the Auger decay of the 3*d* hole states. The ground, 3*d* hole, and final ionic states of the Auger decay are described within the multiconfiguration Dirac-Fock method. In this method, using the rotational symmetry of atoms, the atomic state functions (ASFs) with given total angular momentum (JM) and parity (P) are approximated by a linear combination of pure jj-coupled configuration state functions (CSFs) of the same symmetry:

$$\Psi_\gamma(PJM) = \sum_r c_{\gamma r}\Phi_r(PJM). \tag{1}$$

The relative photoionization cross section from Sr ground state i to the 3*d* hole state β can be expressed, within the frozen core approximation, as

$$Q_\beta(J_\beta) = \frac{1}{3}Q'_\beta(J_\beta)\sum_{l,j}\int |\langle n_\alpha l_\alpha j_\alpha \| r^{(1)} \| \epsilon l j\rangle|^2 d\epsilon, \tag{2}$$

where $n_\alpha l_\alpha j_\alpha$ refers to the $3d_{3/2}$ and $3d_{5/2}$ subshells. The first term is

$$Q'_\beta(J_\beta) = (2j_\alpha+1)\left|\sum_\nu\sum_\alpha c_{\beta\nu}c_{i\alpha}\delta_{X\nu Y\alpha}\right|^2, \tag{3}$$

with X_ν referring to the photoionized 3*d* hole state configuration associated with CSF $\Phi_\nu(J_\beta)$ and Y_α referring to the same parent configuration after coupling the 3*d* orbital from the ground state CSF $\Phi_\alpha(J_i)$. Using linearly polarized light for the photoionization, the relative 3*d* photoelectron intensities are directly proportional to the relative photoionization cross sections given by Eq. (2) if the photoelectrons are detected at the magic angle of 54.7° with respect to the polarization vector of the incident light.

Using the magic angle to detect the emitted Auger electrons following the 3*d* ionization, the relative Auger intensity corresponding the Auger decay from 3*d* hole state β to final ionic state f of the Auger decay can be obtained as

$$n_{f\beta}(J_f,J_\beta) = \frac{T_{f\beta}(J_f,J_\beta)Q_\beta(J_\beta)}{P_\beta(J_\beta)}. \tag{4}$$

In Eq. (4), $P_\beta(J_\beta)$ is the total decay rate, or equivalently, the total decay width of the 3*d* hole state β, and

TABLE I. Configurations used in bound state MCDF calculations.

Ground state	
	$3d^{10}4s^24p^6(4d^2,4d^15s^1,$ $4d^16s^1,5s^2,5s^16s^1,5p^2,6s^2)$
3*d* photoionized state	
step 1:	$3d^94s^24p^64d^2$
step 2:	$3d^94s^24p^6(4d^2,4d^15s^1,$ $4d^16s^1,5s^2,5s^16s^1,5p^2,6s^2)$
Final ionic states of the Auger decay	
A:	$3d^{10}4s^24p^6$
B:	$3d^{10}4s^24p^5(4d^1,5s^1,5p^1,6s^1)$
C:	$3d^{10}4s^14p^6(4d^1,5s^1)$
D:	$3d^{10}4s^24p^4(4d^2,4d^15s^1,5s^2,5p^2,6s^2)$

$$T_{f\beta}(J_f,J_\beta) = 2\pi\sum_{l_A,j_A}\left|\sum_\mu\sum_\nu c_{f\mu}c_{\beta\nu}M^{\mu\nu}_{f\beta}\right|^2 \tag{5}$$

is the Auger rate. In Eq. (5), $M^{\mu\nu}_{f\beta}$ $=\langle\Phi_\mu(J_f)\epsilon_A l_A j_A; J_\beta\|\mathbf{V}\|\Phi_\nu(J_\beta)\rangle$ is the Coulomb matrix element where, on the left side, a continuum electron $|\epsilon_A l_A j_A\rangle$ is coupled to the final ionic ($N-1$ electrons) CSF to form a N-electron scattering state with one electron in the continuum. For more detailed theoretical description of the photoionization and the Auger decay processes see, e.g., Ref. [3].

IV. CALCULATIONS

In the present work, all the bound state ASFs were generated within the MCDF method using the GRASP92 package [13]. The Dirac-Coulomb Hamiltonian was applied in order to define the self-consistent field (SCF) in the computations. Calculations were performed separately for the ground, 3*d* hole, and final ionic states of the Auger decay using the configuration sets presented in Table I. The relative photoionization intensities [Eq. (2)], the total (P_β) and partial Auger decay widths, as well as the relative Auger intensities [Eq. (4)] were determined in the framework of the RATIP package [14,15].

In the MCDF method, a full SCF computation is not often successful if large wave function expansions are involved and especially if some of the orbitals are sensitive (collapse) to an inner vacancy. Because of this difficulty, the calculation of the Sr 3*d* hole state ASFs was performed in two steps, in a way similar to what was done previously for Ba in Ref. [7]. A first series of computations for the Sr 3*d* hole state was already reported in Ref. [6], but the agreement with the experimental PES was not good. By applying these 3*d* hole state expansions, the structures of the AES resulting in the final ionic states A and B deviated drastically from the experimental observations. Due to these discrepancies in the calculated spectra, the 3*d* hole state ASFs were regenerated with respect to Ref. [6] using slightly different configuration

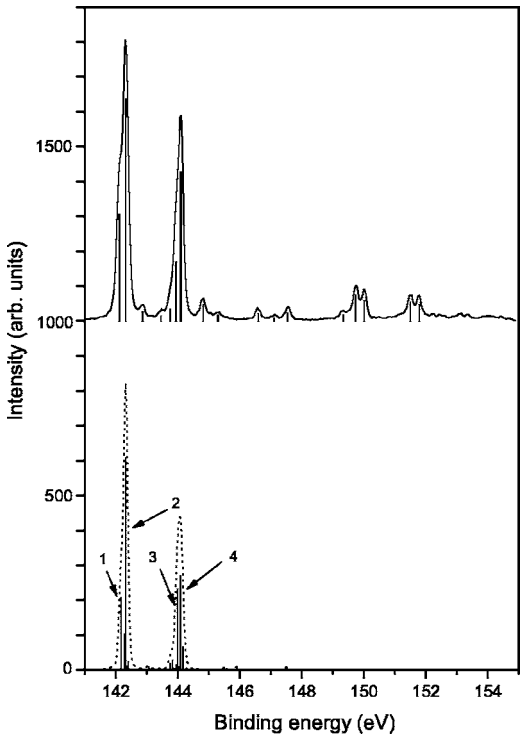

FIG. 1. Experimental (upper part) and calculated Sr 3*d* PES (lower part). For visual comparison with the experiment, the calculated spectrum is plotted using linewidths obtained from the experimental spectrum (dashed line).

sets in order to affect the SCF central field potential and thus to generate somewhat better valence orbitals (4*d*, 5*s*, 5*p*, and 6*s*). First, the step 1 configuration set was used to find good approximations for the inner-shell orbitals (1*s* to 4*p*) when the 4*d* orbitals were present. Second, step 2 configuration set was used with fixed inner-shell orbitals 1*s* to 4*p* from the step 1 calculation. In total, using the step 2 configuration set, 88 ASFs were obtained for the 3*d* hole state with total angular momentum values 3/2 and 5/2. The relative photoelectron intensities were calculated using the photon energy of 255 eV to generate the continuum orbitals ϵlj.

In the final ionic states of the Auger decay, in addition to the the configuration sets A-D presented in Table I, the CSFs with all possible total angular momentum values from the configurations $3d^{10}4s^{0}4p^{6}4d^{2}$, $3d^{10}4s^{0}4p^{6}4d^{1}5s^{1}$, $3d^{10}4s^{0}4p^{6}5s^{2}$, $3d^{10}4s^{0}4p^{6}5p^{2}$, $3d^{10}4s^{1}4p^{5}4d^{2}$, $3d^{10}4s^{1}4p^{5}4d^{1}5s^{1}$, $3d^{10}4s^{1}4p^{5}5s^{2}$, and $3d^{10}4s^{1}4p^{5}5p^{2}$ were also included in the calculation. This was done in order to determine the total Auger decay widths of the 3*d* hole states. In total, 471 final states for the Auger decay were obtained by using these configuration sets.

V. RESULTS AND DISCUSSION

A. Photoionization

The calculated Sr 3*d* PES is presented in Fig. 1 in comparison with the experimental spectrum [6]. The four strongest photoelectron lines are marked in the figure using the numbers 1-4. Lines 1 and 2 are associated with the transitions from ground state to the 3*d* hole states with total angular momentum value $J=5/2$, and lines 3 and 4 with the value $J=3/2$. The 3*d* hole state corresponding to line 1 is dominated by the configuration $3d^{9}4s^{2}4p^{6}4d^{1}5s^{1}$ while in the other states (lines 2-4), the strongest contributions arise from the configuration $3d^{9}4s^{2}4p^{6}5s^{2}$. The relative photoelectron intensities for lines 1-4 are also listed in the first column of Table II in comparison with experimental findings. The present calculation gives quite a good description for the Sr 3*d* photoionization process as is seen by comparing the results to the experimental spectrum. The main lines 1-4 of the PES are especially well reproduced, except for some small discrepancies in the relative intensities. At larger binding energies ($E_b > 145$ eV), the calculation cannot, however, predict completely the experimentally observed satellite structure. The shake-up effect, omitted in the PES calculations, can explain part of the discrepancy between theory and experiment. The calculated overlap integrals between the ground state 5*s* and 3*d* hole state 6*s* orbitals predict shake-up transitions with intensities of about 9% of the main peak intensity. According to our calculations, these shake structures appear at binding energies of about 150 and 152 eV.

B. Total and partial Auger decay widths

Table II shows the calculated total Auger decay widths for the 3*d* hole states 1-4 in comparison with the experimental results obtained by least-squares fitting of the PES. Overall, the total decay widths are in good agreement to the experimental findings and they are also almost the same for the states 1-4. However, according to our calculations, large discrepancies from these values were obtained for the 3*d* hole states corresponding to the weak peaks in the PES at binding energies $E_b > 145$ eV. The strongest contributions to the total

TABLE II. Relative photoelectron intensities [Q_β, Eq. (2)] for the transitions from the Sr ground state to the 3*d* hole states 1-4 (see Fig. 1). Total Auger decay widths P_β for the states 1-4 and their partial Auger decay widths to the final states A-D.

	Relative photoelectron intensity		Total Auger decay width (meV)		Partial Auger decay width (meV)			
Initial state	MCDF	Expt.	MCDF	Expt.	A	B	C	D
1	0.339	0.501	82.36	75±10	0.0038	3.75	0.37	13.23
2	1.000	1.000	82.53	75±10	0.0613	3.64	0.66	12.72
3	0.379	0.335	78.89	75±10	0.0354	2.96	0.48	13.58
4	0.444	0.666	80.15	75±10	0.0082	4.04	0.70	13.41

Auger decay widths originate from Auger decay to the $3d^{10}4s^{0}4p^{6}nln'l'$ and $3d^{10}4s^{1}4p^{5}nln'l'$ final ionic states ($\approx$60–65 meV), but they do not belong to the investigated energy region. These final states are omitted from the analysis since they are overlapping strongly with second step Auger transitions, which does not allow a precise analysis of the first step Auger intensities.

Table II shows also the calculated partial Auger decay widths to the final ionic states A-D for the initial states 1-4. They were determined as a sum over Auger rates [Eq. (5)] from the corresponding initial states to the associated final ionic states. Within the states 1-4 there are some minor differences in the partial Auger decay widths arising from the decay to the final ionic states B-D, but the decay to the final state A (v^{-2}) clearly differs from this finding. For instance, the partial Auger decay width due to the transition to the final state A for the state 2 (0.0613 meV) is about 15 times larger than the corresponding values for the state 1 (0.0038 meV). Similar behavior can also be obtained between the states 3 and 4, but the effect is not so strong. These anomalies in the partial Auger decay widths to the final state A are due to the fact that this decay is described mainly by the distribution of the configuration $3d^{9}4s^{2}4p^{6}4d^{2}$ in the $3d$ hole state expansion, whereas in the Auger decay, where only one or no valence orbitals are involved (final states B-D), the distribution of the configurations $3d^{9}4s^{2}4p^{6}4d^{1}5s^{1}$ and $3d^{9}4s^{2}4p^{6}5s^{2}$ is more important. The main reason for the strong contribution from configuration $3d^{9}4s^{2}4p^{6}4d^{2}$ to the decay to the final state A is certainly the partial collapse of the $4d$ orbital in the photoionization of a $3d$ electron. This gives rise to a large effective interaction strength [16] of the form $X^{k=0}(3d\epsilon d,4d4d)$ and, hence, to a large Auger amplitudes [$c_{f\mu}c_{\beta\nu}M_{f\beta}^{\mu\nu}$ in Eq. (5)]. In addition, if several strongly contributing configurations and especially $3d^{9}4s^{2}4p^{6}(4d,5s)^{2}$ are included in the $3d$ hole state expansions, large Auger amplitudes with negative and positive signs are created, which may lead to destructive or constructive interferences and which are noticeable especially for the initial states 1-4. These effects are also responsible for the discrepancies in the total Auger decay widths of the $3d$ hole states corresponding to the weak peaks in the PES at $E_b > 145$ eV. They are similar to an earlier finding in case of Ba [7], and they also appear in Auger decay to the final states B-D, but the effects are smaller.

C. Auger intensities

The AES to the final ionic states A-D, calculated according to Eq. (4), are shown in Fig. 2 in comparison with the experimental spectrum. The bands corresponding to the Auger decay to the final states A-D are marked on the figure using the notations AES-A through AES-D, respectively. For more detailed analysis of the AES, we also show one by one the AES originating from the $3d$ hole states 1-4. We have not included on the figure the Auger transitions corresponding to the decay to the final states $3d^{10}4s^{0}4p^{6}nln'l'$ and $3d^{10}4s^{1}4p^{5}nln'l'$ ($E_k \approx 0$–60 eV). The experimental spectrum is a combination of two separate spectra measured at photon energies of 190 and 210 eV, whereas in the calculation, the photon energy 255 eV was used. The relative $3d$ photoionization cross sections should not be affected significantly by the photon energy differences between different AES measurements (190 and 210 eV) or between AES and PES (255 eV) measurements, since all the photon energies used are well over the $3d$ ionization threshold thus, the dipole matrix elements in Eq. (2) can be expected to be nearly the same for all transitions regardless of the photon energy used [17].

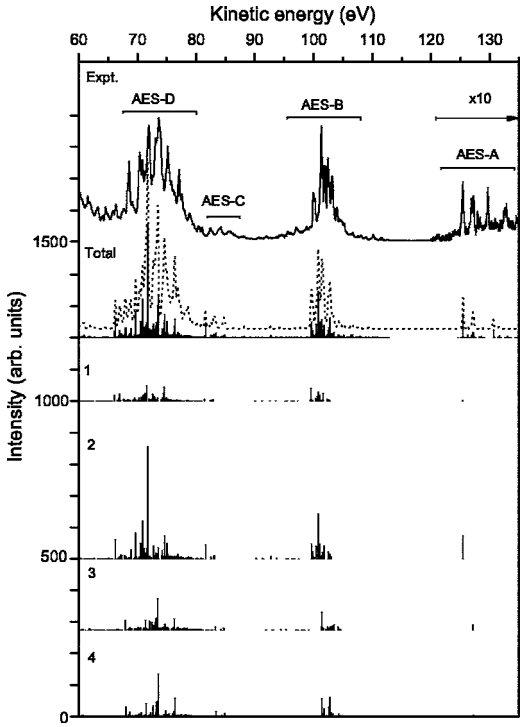

FIG. 2. Experimental (solid line) and calculated (vertical bars) Sr $3d$ AES to the final states A-D. The AES originating from the initial states 1-4 are shown one by one. For visual comparison with the experiment, the calculated AES is plotted using linewidths obtained from experiment (dashed line). The intensities at the energy region $E_k = 120$–135 eV have been multiplied by factor of 10 in each spectrum.

Despite small discrepancies in the relative intensities of the photoelectron peaks and photon energies used, the present calculation predicts the main features of the AES-A through AES-D bands with good accuracy. In AES-A, the calculation even predicts the intense structure at $E_k \approx 131$ eV arising from the decay of the $3d$ hole states corresponding to the weak satellite states in the PES. The intensity distributions of the AES-B (see also Fig. 3), AES-C, and AES-D are also in good overall correspondence to the experiment. However, there are some small discrepancies between the calculation and experiment in AES-B at $E_k \approx 103$ eV, where some structures are missing from the calculated one. In AES-D, the calculation predicts, instead, a slightly too strong line at $E_k \approx 72$ eV. In addition, the relative intensities of the spectra AES-A through AES-D seem to differ a bit from the experimental results, as can be seen from Table III. This discrepancy in the relative intensities is likely caused by the fact that a rather small wave function expan-

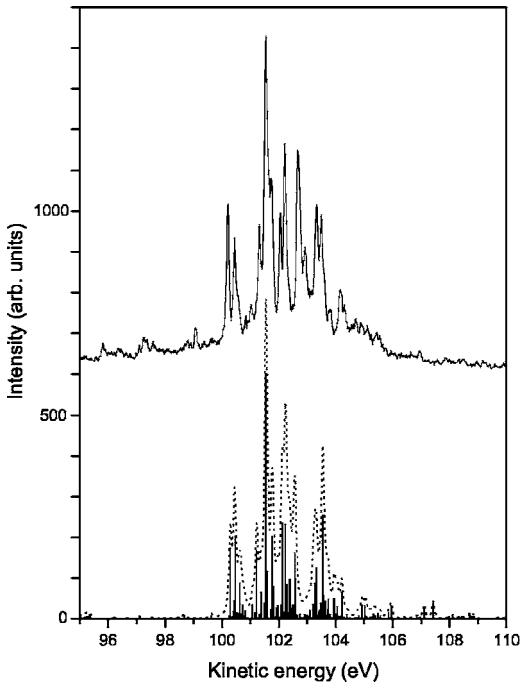

FIG. 3. Experimental (solid line) and calculated (vertical bars) AES-B. For visual comparison with the experiment, the calculated spectrum is plotted using linewidths obtained from experiment (dashed line).

sion had to be used for the representation of the final states, especially in order to describe the final levels for the band AES-D.

Table III displays the contributions from the initial states 1-4 to the bands AES-A through AES-D. Obviously, the AES-A shows the strongest deviation from the other bands. While the total intensity of the other three bands (AES-B, AES-C, and AES-D) amounts to almost 80% from decay of the main 3*d* hole states 1-4, the corresponding value in AES-A is only 55%. There are also large deviations in the contribution of different initial states in the AES-A intensities. For instance, state 2 contributes about three to five times more in the intensity of the bands AES-B through AES-D than the state 1, while the corresponding value in AES-A is about 50. When states 3 and 4 are compared, state 4 contributes slightly more in bands AES-B through AES-D than state 3 but in AES-A, state 3 gives about a four times larger contribution. As discussed above, the different decay properties of the initial states to the final state A are caused by the interference effects in the Auger amplitudes.

TABLE III. Relative intensities of the spectra AES-A through AES-D and the contributions from the initial states 1-4 (see Fig. 1) to the intensities of the corresponding spectra.

	Relative Auger intensities			
	AES-A	AES-B	AES-C	AES-D
MCDF	0.004	0.292	0.047	1.000
Expt.	0.012	0.495	0.039	1.000
	Contributions from the different initial states to the Auger decay (%)			
Initial state				
1	0.9	12.2	7.7	12.6
2	42.2	35.4	39.1	35.7
3	9.6	11.2	11.3	15.1
4	2.6	17.7	19.7	17.2
Other states	44.7	23.5	22.2	19.5

Although there were only some small differences in the partial Auger decay widths within the initial states 1-4 to the final states B-D, the intensity distributions of the corresponding spectra AES-B through AES-D are quite different, as is seen from Fig. 2. This reflects the importance of interference effects in the Auger decay processes as well, where not only the outer valence orbitals are involved (AES-A). However, the effects are more complicated than in the case of AES-A due to the open shell structure in the final states.

VI. CONCLUSIONS

High-resolution experimental studies combined with MCDF calculations for photoionization cross sections and Auger transition rates have allowed us to resolve and to understand the effect of electron-electron correlations in the Sr 3*d* hole state in detail. The 4*d* orbitals experiencing the collapse contribute drastically to the properties of the 3*d* hole state wave functions. This leads to the intensity redistribution in the photoionization and also affects the Auger decay properties of the photoionized 3*d* states. The Auger rates are strongly modified by the interference effects created by the correlated 3*d* hole states especially in the Auger decay resulting in the v^{-2} hole state. This effect is similar to what was obtained for Ba 4*d* Auger transition resulting in the v^{-2} hole state [7]. In addition to the study for Ba, the Auger transitions resulting in the $4p^{-2}$, $4s^{-1}\,v^{-1}$, and $4p^{-1}\,v^{-1}$ final ionic states were also investigated, revealing the importance of interference effects even in Auger transitions where only one or no valence orbitals participate. A complete agreement between the computations and the experiments cannot be achieved, but the main properties of the investigated processes can be understood well. Similar effects can also be expected in the corresponding transitions of Ba. However, the effects cannot be assumed to be exactly the same in Ba, since in Ba, in addition to the 5*d* orbitals, the 4*f* orbitals also experience strong relaxation.

ACKNOWLEDGMENTS

We are grateful to the staff of the MAX and ALS synchrotron laboratories for help during the measurements. Financial support from the National Gradute School in Materials Physics, the European Community Access to Research Infrastructure Action of the Improving Human Potential Programme and the Research Council for the Natural Sciences of the Finnish Academy and the Department of Energy, Office of Science, BES are acknowledged. J. N. would like to acknowledge the Vilho, Yrjö and Kalle Väisälä Foundation, the Oulu University Scholarship Foundation, Magnus Ehrnrooth Foundation, and the Faculty of Sciences, University of Oulu.

[1] W. Mehlhorn, B. Breuckmann, and D. Hausamann, Phys. Scr. **16**, 177 (1977).
[2] W. Weber, B. Breuckmann, R. Huster, W. Menzel, W. Mehlhorn, M. H. Chen, and K. G. Dyall, J. Electron Spectrosc. Relat. Phenom. **47**, 105 (1988).
[3] A. Mäntykenttä, H. Aksela, S. Aksela, J. Tulkki, and T. Åberg, Phys. Rev. A **47**, 4865 (1993).
[4] T. Matila and H. Aksela, J. Phys. B **33**, 653 (2000).
[5] G. Snell, M. Martins, E. Kukk, W. T. Cheng, and N. Berrah, Phys. Rev. A **63**, 062715 (2001).
[6] J. Nikkinen, H. Aksela, S. Heinäsmäki, E. Kukk, N. Berrah, and S. Aksela, Phys. Scr. **T115**, 119 (2005).
[7] J. Nikkinen, H. Aksela, S. Heinäsmäki, S. Fritzsche, E. Kukk, M. Huttula, and S. Aksela, Phys. Rev. A **66**, 064703 (2002).
[8] M. Bässler, J.-O. Forsell, O. Björneholm, R. Feifel, M. Jurvansuu, S. Aksela, S. Sundin, S. L. Sorensen, R. Nyholm, A. Ausmees, and S. Svensson, J. Electron Spectrosc. Relat. Phenom. **101–103**, 953 (1999).
[9] M. Bässler, A. Ausmees, M. Jurvansuu, R. Feifel, J.-O. Forsell, P. de Tarso Fonseca, A. Kivimäki, S. Sundin, S. L. Sorensen, R. Nyholm, O. Björneholm, S. Aksela, and S. Svensson, Nucl. Instrum. Methods Phys. Res. A **469**, 382 (2001).
[10] J. Jauhiainen, A. Ausmees, A. Kivimäki, S. J. Osborne, A. Naves de Briton, S. Aksela, S. Svensson, and H. Aksela, J. Electron Spectrosc. Relat. Phenom. **69**, 181 (1994).
[11] T. X. Carroll, J. D. Bozek, E. Kukk, V. Myrseth, L. J. Saethre, T. D. Thomas, and K. Wiesner, J. Electron Spectrosc. Relat. Phenom. **125**, 127 (2002).
[12] G. C. King, M. Tronc, F. H. Read, and R. C. Bradford, J. Phys. B **10**, 2479 (1977).
[13] F. A. Parpia, C. Froese Fisher, and I. P. Grant, Comput. Phys. Commun. **94**, 249 (1996).
[14] S. Fritzsche, J. Electron Spectrosc. Relat. Phenom. **114–116**, 1155 (2001).
[15] J. Nikkinen, S. Fritzsche, and S. Heinäsmäki (to be published).
[16] S. Fritzsche, C. Froese Fischer, and G. Gaigalas, Comput. Phys. Commun. **148**, 103 (2002).
[17] M. Huttula, E. Kukk, S. Heinäsmäki, M. Jurvansuu, S. Fritzsche, H. Aksela, and S. Aksela, Phys. Rev. A **69**, 012702 (2004).